Laser wakefield acceleration of electrons with ionization injection in a pure N5+ plasma waveguide

A. J. Goers, S. J. Yoon, J. A. Elle, G. A. Hine, and H. M. Milchberg

Citation: Applied Physics Letters **104**, 214105 (2014); doi: 10.1063/1.4880102
View online: http://dx.doi.org/10.1063/1.4880102
View Table of Contents: http://scitation.aip.org/content/aip/journal/apl/104/21?ver=pdfcov
Published by the AIP Publishing

Laser wakefield acceleration of electrons with ionization injection in a pure N^{5+} plasma waveguide

A. J. Goers, S. J. Yoon, J. A. Elle, G. A. Hine, and H. M. Milchberg
Institute for Research in Electronics and Applied Physics, University of Maryland, College Park, Maryland 20742, USA

(Received 29 April 2014; accepted 14 May 2014; published online 30 May 2014)

Ionization injection-assisted laser wakefield acceleration of electrons up to 120 MeV is demonstrated in a 1.5 mm long pure helium-like nitrogen plasma waveguide. The guiding structure stabilizes the high energy electron beam pointing and reduces the beam divergence. Our results are confirmed by 3D particle-in-cell simulations. © *2014 AIP Publishing LLC*. [http://dx.doi.org/10.1063/1.4880102]

Laser wakefield acceleration (LWFA) is an attractive and widely used scheme employing the ~GeV/cm accelerating gradients produced in a laser-driven plasma wake.[1,2] Recently, several groups have reported LWFA of electrons to energies >2 GeV using petawatt-scale drive lasers.[3] Efficient acceleration of electrons to high energies under LWFA requires matching the accelerator length to the dephasing length, L_d, with maximum single stage energy gains scaling as $N_e^{-2/3}$, where N_e is the plasma electron density.[4,5] Often this requires self-guiding of the drive laser pulse over distances many times the Rayleigh range through relativistic self-focusing, requiring laser powers exceeding the critical power, $P_{cr} = 17(N_{cr}/N_e)\ GW$.[2] Thus, although the maximum energy gain increases for lower density, P_{cr} increases and quickly exceeds what can be achieved by a typical table-top laser system. Alternatively, high intensity laser interaction with the plasma can be extended through the use of a plasma waveguide, which provides a refractive index structure capable of guiding the drive pulse with a small spot size over many Rayleigh lengths.[6] The use of plasma channels has been shown to improve stability of wakefield accelerated high energy electron beams and offers independent control over the guiding and acceleration processes.[7,8] The acceleration of electrons to >1 GeV has been achieved using preformed channels produced in a capillary discharge waveguide with a relatively modest 40 TW peak power.[9]

Another critical issue for the advancement of wakefield accelerators is the control of electron injection into the accelerating phase of the plasma wake.[5] Seeding of electrons into the wakefield can naturally occur when the amplitude of the plasma wave reaches the wave breaking limit, typically requiring drive pulses with normalized vector potential $a_0 \gg 1$ or high plasma densities. Other schemes involving multiple pulses[10,11] or tailored plasma density profiles[12,13] to control injection of background electrons into the wake have been proposed to create tunable wakefield accelerators. Recently, ionization injection of high Z dopants was proposed and demonstrated to increase electron beam charge and lower the intensity threshold for electron trapping.[14–20] In this scheme, inner shell electrons of a high Z dopant are ionized near the peak of the drive laser pulse and are trapped in the potential well of the plasma wave. In the previous experiments, the high-Z dopant typically does not exceed ~10% of the total density due to laser pulse refraction by the additional plasma density created on axis.[20]

In this work, we demonstrate ionization injection-assisted LWFA in a pure He-like nitrogen (N^{5+}) plasma waveguide. We show that use of a preformed plasma channel with a guiding structure stabilizes and narrows the accelerated electron beam compared to the use of a broad density profile. The trapping and acceleration processes in the N^{5+} plasma channel are confirmed by 3D particle-in-cell (PIC) simulations.

Figure 1(a) is a schematic of the experimental setup. Two types of preformed plasmas were generated in a nitrogen cluster jet pulsed at 10 Hz. Plasma waveguides were generated by focusing a 10 Hz Nd:YAG laser pulse (1064 nm, 140 ps, 400 mJ)

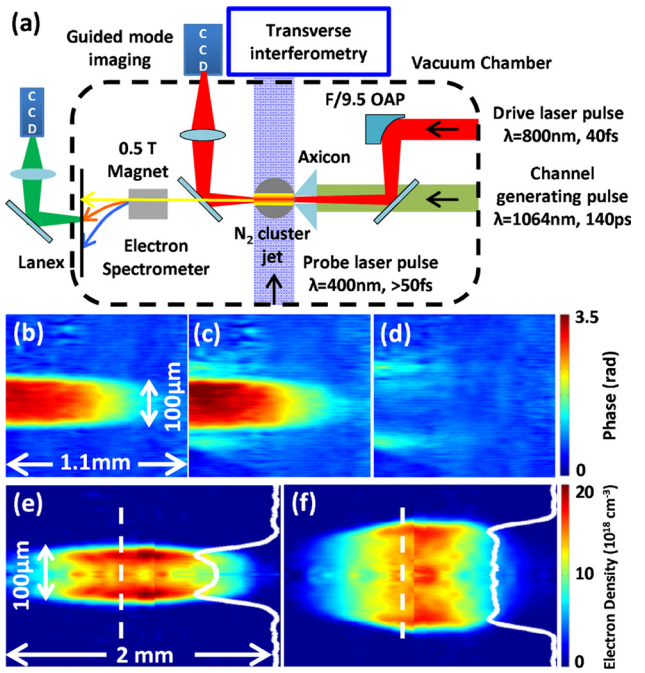

FIG. 1. (a) A schematic of the experimental setup used to create plasma waveguides in a nitrogen cluster target. A flat plasma profile was also created by focusing the channel-generating pulse onto the cluster jet with an f/20 lens (not shown) through the final drive pulse turning mirror. Phase profiles at the waveguide exit before (b) and after (c) guiding of a 0.4 TW pulse show additional ionization only outside the plasma waveguide; (d) is the difference between (c) and (b). Abel inversion of the phase images allowed reconstruction of the waveguide (e) and flat (f) plasma density profiles, with lineouts along the white dashed lines shown on the right sides of the panels.

with an axicon to a tight ~1 cm line focus overlapping the 1.5 mm jet width. Much broader plasma channels, with a nearly flat transverse density profile, were generated by focusing ~100 mJ into the jet with an f/20 lens. The target length of 1.5 mm is approximately equal to the dephasing length for a $1.1 \times 10^{19}\,\mathrm{cm}^{-3}$ density plasma.

Clusters form in our jet as high pressure gas expands into vacuum, with Van der Waals forces forming aggregates at solid density with typical radii between 1 and 100 nm, controlled by the gas backing pressure, species, valve temperature, and nozzle geometry.[21,22] In our experiments, the cluster jet valve body was cryogenically cooled to 100 K, with valve backing pressure in the range 200–400 psi. Our previous study showed that the monomer contribution in the nitrogen cluster jet drops significantly at these conditions.[23] We control the plasma density by tuning the backing pressure and jet opening time. We have also previously shown that our ~100 ps channel-forming laser pulses can be absorbed by cluster jets with an efficiency of ~50%.[24] The ionized and heated clusters expand and merge over ~10 ps timescale to form a locally uniform plasma which then expands, driving a cylindrical shockwave at the boundary between the plasma and neutral clusters. After >100 ps delay a concave radial plasma profile develops, suitable for guiding of an injected high intensity laser pulse.[25]

Our LWFA driver was an 800 nm, 40 fs Ti:sapphire laser pulse focused by a f/9.5 off-axis parabolic mirror (OAP) and steered by an 800 nm mirror to a 15 μm FWHM spot, with a peak normalized vector potential $a_0 = 1.2$. The drive pulse was synchronized with the plasma channel-forming pulse with less than 10 ps jitter and injected collinear to the plasma axis at an adjustable delay with respect to channel formation. For experiments with the plasma waveguide, the drive pulse was focused through a hole in the axicon, as shown in Fig. 1(a). For experiments with the flat plasma profile, the 1064 nm pulse was focused by a lens through the 800 nm turning mirror and onto the cluster target.

For time-resolved interferometry of the cluster jet and the plasma, a small portion of the Ti:sapphire laser pulse was split from the main beam, frequency doubled, and directed transversely across the jet to a folded wavefront interferometer and onto a CCD. Phase extraction followed by Abel inversion allowed reconstruction of the channel density profile assuming cylindrical symmetry.[26] Adjusting the probe pulse timing enabled interferometry of the neutral gas as well as the plasma channel before and after passage of the LWFA driver pulse. Using a translatable mirror (moved for electron measurements), the driver beam mode exiting the plasma was imaged onto a CCD camera and its spectrum was monitored. Electron beam profiles and energy spectra were measured using an electron spectrometer consisting of a 2 in. long 0.5 T NdFeB magnet and a Lanex[27] screen. The screen was placed 15 in. from the cluster jet and 10 in. from the end of the magnet. A 100 μm thick aluminum foil was placed before the Lanex screen to shield it from the laser beam, and a green filter was placed in front of the CCD to improve the signal to noise ratio.

Cluster sources have been shown to be very efficient targets for plasma channel formation.[24,28] Collisional ionization within the solid density clusters at the leading edge of the channel forming pulse creates significantly more ionized plasma than an unclustered gas jet of the same average density. This highly ionized plasma is then efficiently heated through inverse bremsstrahlung over the full duration of the long (140 ps) channel forming pulse,[25] typically resulting in dominant populations of closed shell ions, for example, Ne-like argon,[28] or in this experiment, He-like nitrogen.

The dominant He-like ionization state of our nitrogen plasma was verified by guiding a 15 mJ, 40 fs (0.4 TW) Ti:sapphire laser pulse in the plasma waveguide. The guide exit mode peak intensity was $10^{17}\,\mathrm{W/cm}^2$, containing 80% of the injected pulse energy. Considering that the ionization threshold of Li-like N^{4+} (ionization potential 98 eV) ions is $\sim 10^{16}\,\mathrm{W/cm}^2$,[29] any Li-like nitrogen ions in the channel would be ionized by the guided pulse, resulting in a increase in electron density easily detectable by interferometry. Figure 1 shows probe phase profiles near the exit of the plasma waveguide, taken before (b) and after (c) guiding of the 0.4 TW pulse. Figure 1(d) is the difference between (b) and (c) and would reveal any extra ionization by the guided pulse. It is seen that the only additional ionization occurs outside the waveguide, where uncoupled laser energy interacts with neutral clusters, verifying that the plasma channel interior is dominated by N^{5+}. As an added check on the ionization state, the measured nitrogen molecule densities were approximately 10 times less than the average plasma densities, indicating 5× ionization of each nitrogen atom.

Figures 1(e) and 1(f) show the electron density profiles of plasmas generated by the axicon-based (e) and lens-based (f) methods described earlier. The lens-generated plasma has a plateau in the center whereas the axicon created plasma has a narrower and well-defined waveguiding structure. An image of this waveguide's low intensity exit mode, with spot size FWHM of 14 μm, is shown in Figure 2(b), in agreement with the calculated mode for this index profile. The low intensity exit mode shows guiding over approximately 2.5 Rayleigh lengths. By tuning the gas jet backing pressure and valve opening time, the peak on-axis density for both cases was set to $1.4 \times 10^{19}\,\mathrm{cm}^{-3}$. Both channels have long density ramps along the laser propagation axis which follow the

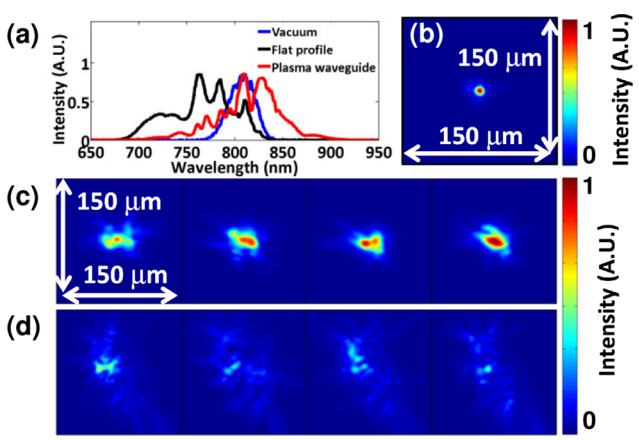

FIG. 2. (a) Optical spectra of the 10 TW laser pulse (vacuum spectrum: blue curve) after interaction in the N^{5+} flat profile channel (black curve) and in the N^{5+} waveguide (red curve). (b) A low intensity (0.4 TW) exit mode (14 μm FWHM) of the plasma waveguide. Exit modes of 10 TW laser pulses imaged at the end of (c) the plasma channel and (d) the flat density profile.

neutral N_2 molecule density profile. PIC simulations presented later show that the density gradient at the end of the channel helps to trap the ionized inner-shell electrons by expanding the plasma bucket, as has been reported earlier.[12]

A 10 TW drive laser pulse with a peak intensity of 3.3×10^{18} W/cm^2 ($a_0 = 1.2$) at the focus was injected into both pre-formed plasma density profiles. Figure 2(a) shows optical spectra of the drive pulse after exiting the flat and waveguide profiles. The spectrum from the waveguide shows a significant red wing, consistent with pulse self-phase modulation over the guide length by a large amplitude plasma wave,[30] while the spectrum from the flat profile is largely blue-shifted due to significant interaction of the drive pulse with unionized clusters outside the flat plasma profile. Laser pulse exit mode images from the waveguide (Fig. 2(c)) show stable shot-to-shot confinement, although relativistic contribution to the guide index profile distorts the mode compared to Fig. 2(b). By contrast, the beam from the flat profile (Fig. 2(d)) is not stable and shows a tight, relativistically self-focused spot that varies shot-to-shot along with significant unfocused energy outside of the flat plasma region. Interaction of the unfocused energy with unionized clusters explains the largely blue-shifted spectrum. This shows that even though the peak laser power satisfies $P/P_{cr} > 3$ at the channel center, under our conditions the plasma waveguide is more effective than relativistic self-focusing in confining laser pulse energy to the propagation axis. This enables the waveguided pulse to drive a large amplitude plasma wave over a longer distance, resulting in the significant redshift missing in the flat plasma case.

The superior drive pulse guiding and redshifting in the plasma waveguide are also manifested in the quality and stability of the accelerated electron beams. Figure 3 shows electron beam profiles from the waveguide plasma, (a), and from the flat channel, (b). The electron beam from the plasma waveguide is both more tightly collimated (2.8 mrad shot-averaged divergence vs. 6.6 mrad from the flat channel) and more stable (12 mrad standard deviation in beam pointing vs. 42 mrad). The charge in the tightly collimated, energetic electron beams of (a) is estimated to be approximately 5 pC based on prior calibration of the Lanex fluorescence[27] and estimated efficiency of the imaging system.

For the plasma waveguide, we observed a quasi-monoenergetic peak as large as 120 MeV (d), with average peak energy ~65 MeV (c), with a low energy tail extending down to 32 MeV. The low energy tail is commonly observed in ionization injection from continuous injection throughout the acceleration process.[14,18–20] For the flat channel, however, we were not able to measure the electron energy due to unstable beam pointing through the magnetic spectrometer.

To gain insight into the trapping and acceleration processes in the N^{5+} plasma waveguide, we performed 3D particle-in-cell simulations using the code TurboWAVE,[31] which includes a tunneling ionization model.[29] In order to assess the contribution of ionization injection from N^{5+} ions in the waveguide, simulations were performed for (*i*) a helium-like nitrogen plasma waveguide and (*ii*) a pre-ionized hydrogen channel with the same electron density profile as (*i*). A $\lambda = 800$ nm, 40 fs, 3.3×10^{18} W/cm^2 peak intensity pulse, with a 14 μm FWHM beam waist was guided in both the N^{5+} and H^+ plasma waveguides. Corresponding to the measured waveguide profile of Fig. 1(e), each end of the simulated channel had an initial 700 μm linear density ramp with on-axis densities rising from 8×10^{18} cm^{-3} to 1.4×10^{19} cm^{-3}, with a 100 μm plateau region in the middle. A short 50 μm ramp at either end brought the plasma density to vacuum. The total charge was neutralized by distributing either N^{5+} or H^+ ions within the channel.

Electron beams similar to those observed experimentally, though with substantially higher charge, were produced from the simulated helium-like nitrogen plasma channel. A mono-energetic peak appears at 80 MeV with a long low energy tail, as can be seen in the phase space plots Figs. 4(c) and 4(d). We can see the trapped electrons inside the bucket in Fig. 4(a), which shows a charge density plot near the end

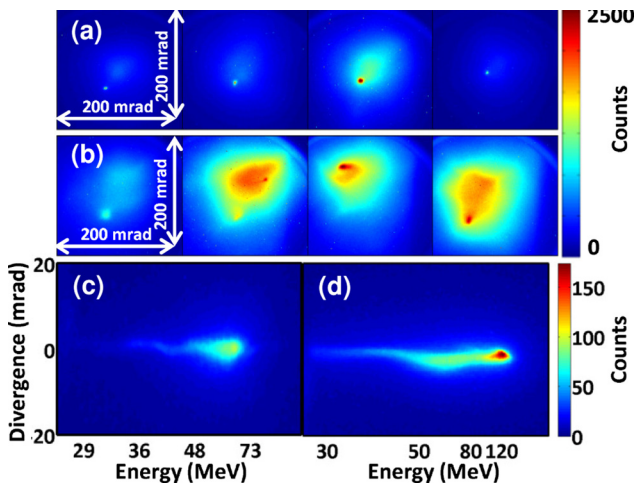

FIG. 3. Electron signals from the Lanex screen without the deflecting 0.5 T magnet generated from (a) the N^{5+} waveguide and (b) the N^{5+} flat density profile. (c) Typical energy spectrum of an electron beam generated in the N^{5+} waveguide. (d) Highest energy spectrum produced from the waveguide profile.

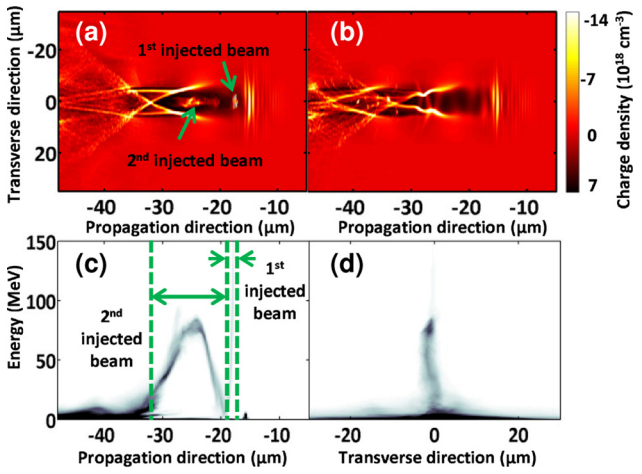

FIG. 4. Charge density plots in a moving window after 1.4 mm propagation in (a) a He-like nitrogen plasma channel showing two trapped electron beams and (b) a pure hydrogen plasma waveguide showing no trapped electrons. (c) Longitudinal (integrated over the transverse directions) and (d) transverse (integrated over the longitudinal direction) phase space plots of the electrons ionized from N^{5+} to N^{6+} in the N^{5+} channel after 1.4 mm propagation.

of the N^{5+} channel. In contrast, in Fig. 4(b), we show that no significant trapping occurs in the hydrogen plasma channel.

Figures 4(a) and 4(c) also show that two spatially separated beams are trapped. The first beam has a lower charge (14 pC) and a broad spectrum extending up to 150 MeV, whereas the second beam contains much more charge (55 pC) and the energy distribution has a quasi-monoenergetic peak at 80 MeV. From the simulations, we observe that the second beam is trapped at the density down ramp, whereas the first beam is trapped starting from the entrance of the channel. Due to the significant difference in accelerated charge observed between the experiment and simulations, only the down ramp injected electrons are seen in the experimental electron spectra. The density down ramp traps significant charge in a short time by expanding the plasma bucket, giving rise to the quasi-monoenergetic peak. Even with the density down ramp, the plasma wave driven by the laser pulse was not strong enough to self-trap background plasma electrons without the help of ionization injection, and simulations showed that both beams are composed of K-shell electrons ionized near the peak of the drive laser pulse.

In conclusion, we have demonstrated ionization-injected LWFA in a pure He-like nitrogen plasma waveguide produced from a cryogenic cluster jet. Guided drive pulses produce electron beams with improved divergence and pointing stability as compared to drive pulses injected into flat, preformed helium-like nitrogen plasmas. Three dimensional PIC simulations verify that ionization injection of K-shell electrons from the abundant helium-like nitrogen ions is essential for trapping and acceleration of relativistic electrons in the waveguide.

This work was supported by the Defense Threat Reduction Agency (DTRA), the U.S. Department of Energy (DoE), and the National Science Foundation (NSF). The authors thank John Palastro for useful discussions and Dan Gordon for use of the code TurboWave.

[1]T. Tajima and J. Dawson, Phys. Rev. Lett. **43**, 267 (1979).
[2]P. Sprangle, E. Esarey, and A. Ting, Phys. Rev. Lett. **64**, 2011 (1990).
[3]X. Wang, R. Zgadzaj, N. Fazel, Z. Li, S. A. Yi, X. Zhang, W. Henderson, Y.-Y. Chang, R. Korzekwa, H.-E. Tsai, C.-H. Pai, H. Quevedo, G. Dyer, E. Gaul, M. Martinez, A. C. Bernstein, T. Borger, M. Spinks, M. Donovan, V. Khudik, G. Shvets, T. Ditmire, and M. C. Downer, Nat. Commun. **4**, 1 (2013); H. T. Kim, K. H. Pae, H. J. Cha, I. J. Kim, T. J. Yu, J. H. Sung, S. K. Lee, T. M. Jeong, and J. Lee, Phys. Rev. Lett. **111**, 165002 (2013).
[4]W. Lu, M. Tzoufras, C. Joshi, F. S. Tsung, W. B. Mori, J. Vieira, R. A. Fonseca, and L. O. Silva, Phys. Rev. Spec. Top. - Accel. Beams **10**, 061301 (2007).
[5]E. Esarey, C. B. Schroeder, and W. P. Leemans, Rev. Mod. Phys. **81**, 1229 (2009).
[6]C. G. Durfee and H. M. Milchberg, Phys. Rev. Lett. **71**, 2409 (1993).
[7]T. P. A. Ibbotson, N. Bourgeois, T. P. Rowlands-Rees, L. S. Caballero, S. I. Bajlekov, P. A. Walker, S. Kneip, S. P. D. Mangles, S. R. Nagel, C. A. J. Palmer, N. Delerue, G. Doucas, D. Urner, O. Chekhlov, R. J. Clarke, E. Divall, K. Ertel, P. S. Foster, S. J. Hawkes, C. J. Hooker, B. Parry, P. P. Rajeev, M. J. V. Streeter, and S. M. Hooker, Phys. Rev. Spec. Top. - Accel. Beams **13**, 031301 (2010).
[8]C. G. R. Geddes, C. Toth, J. van Tilborg, E. Esarey, C. Schroeder, D. Bruhwiler, C. Nieter, J. Cary, and W. P. Leemans, Nature **431**, 538 (2004).
[9]W. P. Leemans, B. Nagler, A. J. Gonsalves, C. Tóth, K. Nakamura, C. G. R. Geddes, E. Esarey, C. B. Schroeder, and S. M. Hooker, Nat. Phys. **2**, 696 (2006).
[10]E. Esarey, R. F. Hubbard, W. P. Leemans, A. Ting, and P. Sprangle, Phys. Rev. Lett. **79**, 2682 (1997).
[11]J. Faure, C. Rechatin, A. Norlin, A. Lifschitz, Y. Glinec, and V. Malka, Nature **444**, 737 (2006).
[12]C. G. R. Geddes, K. Nakamura, G. R. Plateau, C. Toth, E. Cormier-Michel, E. Esarey, C. B. Schroeder, J. R. Cary, and W. P. Leemans, Phys. Rev. Lett. **100**, 215004 (2008).
[13]A. J. Gonsalves, K. Nakamura, C. Lin, D. Panasenko, S. Shiraishi, T. Sokollik, C. Benedetti, C. B. Schroeder, C. G. R. Geddes, J. van Tilborg, J. Osterhoff, E. Esarey, C. Toth, and W. P. Leemans, Nat. Phys. **7**, 862 (2011).
[14]E. Oz, S. Deng, T. Katsouleas, P. Muggli, C. D. Barnes, I. Blumenfeld, F. J. Decker, P. Emma, M. J. Hogan, R. Ischebeck, R. H. Iverson, N. Kirby, P. Krejcik, C. O'Connell, R. H. Siemann, D. Walz, D. Auerbach, C. E. Clayton, C. Huang, D. K. Johnson, C. Joshi, W. Lu, K. A. Marsh, W. B. Mori, and M. Zhou, Phys. Rev. Lett. **98**, 084801 (2007).
[15]T. P. Rowlands-Rees, C. Kamperidis, S. Kneip, A. J. Gonsalves, S. P. D. Mangles, J. G. Gallacher, E. Brunetti, T. Ibbotson, C. D. Murphy, P. S. Foster, M. J. V. Streeter, F. Budde, P. A. Norreys, D. A. Jaroszynski, K. Krushelnick, Z. Najmudin, and S. M. Hooker, Phys. Rev. Lett. **100**, 105005 (2008).
[16]A. Pak, K. A. Marsh, S. F. Martins, W. Lu, W. B. Mori, and C. Joshi, Phys. Rev. Lett. **104**, 025003 (2010).
[17]C. McGuffey, A. G. R. Thomas, W. Schumaker, T. Matsuoka, V. Chvykov, F. J. Dollar, G. Kalintchenko, V. Yanovsky, A. Maksimchuk, K. Krushelnick, V. Y. Bychenkov, I. V. Glazyrin, and A. V. Karpeev, Phys. Rev. Lett. **104**, 025004 (2010).
[18]Y.-C. Ho, T.-S. Hung, C.-P. Yen, S.-Y. Chen, H.-H. Chu, J.-Y. Lin, J. Wang, and M.-C. Chou, Phys. Plasmas **18**, 063102 (2011).
[19]M. Z. Mo, A. Ali, S. Fourmaux, P. Lassonde, J. C. Kieffer, and R. Fedosejevs, Appl. Phys. Lett. **100**, 074101 (2012).
[20]M. Z. Mo, A. Ali, S. Fourmaux, P. Lassonde, J. C. Kieffer, and R. Fedosejevs, Appl. Phys. Lett. **102**, 134102 (2013).
[21]O. Hagena, Surf. Sci. **106**, 101 (1981).
[22]K. Y. Kim, V. Kumarappan, and H. M. Milchberg, Appl. Phys. Lett. **83**, 3210 (2003).
[23]S. J. Yoon, A. J. Goers, G. A. Hine, J. D. Magill, J. A. Elle, Y.-H. Chen, and H. M. Milchberg, Opt. Express **21**, 15878 (2013).
[24]H. Sheng, K. Y. Kim, V. Kumarappan, B. D. Layer, and H. M. Milchberg, Phys. Rev. E **72**, 036411 (2005).
[25]V. Kumarappan, K. Y. Kim, and H. M. Milchberg, Phys. Rev. Lett. **94**, 205004 (2005).
[26]T. R. Clark and H. M. Milchberg, Phys. Rev. Lett. **78**, 2373 (1997).
[27]A. Buck, K. Zeil, A. Popp, K. Schmid, A. Jochmann, S. D. Kraft, B. Hidding, T. Kudyakov, C. M. S. Sears, L. Veisz, S. Karsch, J. Pawelke, R. Sauerbrey, T. Cowan, F. Krausz, and U. Schramm, Rev. Sci. Instrum. **81**, 033301 (2010).
[28]H. M. Milchberg, K. Y. Kim, V. Kumarappan, B. D. Layer, and H. Sheng, Philos. Trans. A. Math. Phys. Eng. Sci. **364**, 647 (2006).
[29]M. V. Ammosov, N. B. Delone, and V. P. Krainov, Sov. Phys. JETP **64**, 1191 (1986).
[30]S. Shiraishi, C. Benedetti, A. J. Gonsalves, K. Nakamura, B. H. Shaw, T. Sokollik, J. van Tilborg, C. G. R. Geddes, C. B. Schroeder, C. Tóth, E. Esarey, and W. P. Leemans, Phys. Plasmas **20**, 063103 (2013).
[31]D. F. Gordon, IEEE Trans. Plasma Sci. **35**, 1486 (2007).